Precision Agriculture (2022) 23:1–17
https://doi.org/10.1007/s11119-021-09823-w

Estimation of nitrogen status of paddy rice at vegetative phase using unmanned aerial vehicle based multispectral imagery

Yi-Ping Wang[1] · Yu-Chieh Chang[1] · Yuan Shen[1,2]

Accepted: 26 May 2021 / Published online: 3 June 2021
© The Author(s), under exclusive licence to Springer Science+Business Media, LLC, part of Springer Nature 2021

Abstract
Precision nitrogen fertilizer application depends on accurate estimation of plant nitrogen content. However, the assessment of plant nitrogen content at early growth stages of paddy rice through remote sensed images is complicated by the compound effects of backgrounds (e.g. flood water, bare soil, algae, etc.) on the band reflectance. The rapid changing of plant nitrogen content during the vegetative phase makes the development of an operational prediction model very difficult. In this study, aerial images acquired by a quadcopter unmanned aerial vehicle (UAV) equipped with a multispectral sensor were used to estimate plant nitrogen content at vegetative phase of rice crops. The experiments were conducted at the experimental farm of Taiwan Agricultural Research Institute (TARI) from 2018 to 2020. A variable, N-index (ratio between N content of plants to be evaluated and plants not receiving N fertilizers), was introduced to resolve the issues related to rapid changing of plant N content during the vegetative phase. After removing the interference on band reflectance by background from the aerial images, the most appropriate vegetation indices and period that can capture the variations of N-index of rice plants were identified. It was found that a normalized difference red edge index (NDRI) and red edge chlorophyll index (RECI) based model correlated well with the N-index values from c.a. 30 days after transplanting (DAT) to 55 DAT (i.e., the most crucial period for rice yield and grain quality). The developed model was then used to display the spatial and temporal heterogeneity in plant nitrogen status within an experimental field as an example to illustrate how to use the model. In the example, soil plant analysis development (SPAD) meter values at locations of various levels of estimated N-index were collected as surrogates of plant nitrogen content at various DATs to build relationships for converting N-index maps to SPAD maps for potential variable rate fertilizer application management.

Keywords UAV · SPAD · Nitrogen · Vegetation indices · Paddy rice

✉ Yuan Shen
yshen@nchu.edu.tw

[1] Department of Soil and Environmental Sciences, National Chung-Hsing University, Taichung, Taiwan, ROC

[2] Innovation and Development Center of Sustainable Agriculture, National Chung-Hsing University, Taichung, Taiwan, ROC

Introduction

Nitrogen (N) is vital to promote rapid rice plant growth and improve yield and grain quality, especially in intensive agricultural systems. (Lee et al., 2011; Wang et al., 2016; Ye et al., 2013). However, environmental and ecological conditions are severely affected by the excess reactive N caused by over and/or improper application of nitrogenous fertilizers (Buresh et al., 1993; Galloway & Cowling, 2002; Ju et al., 2006). Matching fertilizer N supply with actual crop demand, thus maximizing crop N uptake and reducing N losses to the environment, is one of the strategic goals of site-specific nutrient management or precision agriculture (Cassman et al., 2002; Raun et al., 2002). Therefore, the ability to provide timely information regarding spatial distribution of crop N status within the field is one of the key factors in implementing precision agriculture (Lee et al., 2008).

Various methods can be used to measure plant N content (Muñoz-Huerta et al., 2013). For example, Kjeldahl-digestion method (Kalra, 1998) is based on laboratory analysis and considered a method of reference for biological sample nitrogen estimation, but it is also laborious, time-consuming, and destructive. Soil plant analyses development meter (SPAD meter) is an instrument commonly used for determination of plant N status on site in fields (e.g. Cabangon et al., 2011; Lin et al., 2010). SPAD meter measures chlorophyll content, which highly correlates with N content in leaves. It is non-destructive but still time-consuming because a SPAD meter only measures leaf N content one leaf at a time. Other than the leaf selected for measurement and measuring positions on the leaf, SPAD meter readings can also be affected by plant growth stage, cultivars, soil water and deficiency of nutrients other than N (Cabangon et al., 2011; Lin et al., 2010). Remote sensing-based solutions have also been used to monitor N status of rice plants (Lee et al., 2008; Stroppiana et al., 2009; Zhu et al., 2008). Determining plant N status by remote sensing techniques is much more appealing than the traditional destructive chemical analyses considering the cost and time required. This technique is also better than using SPAD meters because there is no need to attach the sensor on the leaf and it can reduce variability of the measurements by adjusting the band reflectance sampling area. In addition, while SPAD measurements are usually taken only on a few plants near the edges of a field, remote sensed images can provide spatial information regarding plant N status of entire field.

In Taiwan, rice seedlings grown in a mat nursery are generally transplanted into puddled and leveled fields 12 to 15 days after seeding, primarily for better weed control. After recovering from the transplanting shock, leaves continue to develop at the rate of one every 3–4 days during the early vegetative phase. The late vegetative phase starts from the appearance of the first tiller. The stem begins to lengthen late in the tillering stage and stops growing in height just before panicle initiation, which also signals the end of the vegetative phase. The number of days that the entire vegetative phase takes varies depending on the variety of rice and crop season, but is typically between 55 and 85 days.

Generally, 25% to 40% of nitrogen fertilizer is applied during the field preparation stage as basal fertilizer, and the rest is split into 2 to 3 portions and top dressed during the vegetative phase with the last portion applied just before panicle initiation. Wang et al. (2012) and Wang and Shen (2015) were able to delineate management zones for site-specific basal fertilizer application through identifying limiting soil factors of each paddy rice field within studied regions. Lee et al. (2008) were able to assess N concentration of rice plants at panicle initiation stage by an inexpensive imaging system mounted on a helicopter (Lee et al., 2007). Techniques to determine rice plant N concentration during vegetative phase are lacking for top dressing N fertilizers in a more

precise manner. However, in the vegetative phase, nitrogen content of rice plants usually varies between 1 and 4% depending mainly on the growth stages and also the time of top dressing the N fertilizers. Therefore, the ability to provide timely information regarding the spatial distribution and temporal changes of plant N content in the field is very important in designing a feasible variable rate N fertilizer application strategy.

During the entire vegetative phase, paddy fields are not fully covered by rice plants until they reach the maximum tillering stage. The compound effects of rice plants and backgrounds (such as water, soil, and sometimes algae) on measured canopy reflectance spectrum result in a commonly observed rapid increase of NDVI values from transplanting and gradually level off near maximum tillering stage (Chang et al., 2005; Wang et al., 2010). Therefore, it is important to be able to remove the interferences of backgrounds from band reflectance of remote sensed images in order to correctly estimate the plant nitrogen content. Linear mixture model (LMM) approaches are commonly used to decompose the band reflectance to reflectance of each composing land surface type (Keshava & Mustard, 2002). The principal assumption of LMM is that the measured reflectance of a pixel is the linear sum of the reflectance of the mixture components, also called endmembers, that make up that pixel. It is also assumed that each endmember has a relatively constant reflectance across the whole scene. The implication is that this approach assumes all the rice plants have the same reflectance spectrum and disregards the spatial heterogeneity of plant nitrogen contents within the field and the corresponding morphological changes. Therefore, the linear mixture model approach may not be suitable from the stand point of implementing variable rate fertilization on site.

Flying at low altitude, unmanned aerial systems (UAS) can acquire images with spatial resolution high enough to separate rice plants from backgrounds. UAS can also provide timely images at very low cost compared with airborne and satellite sensors. Zheng et al. (2018) evaluated the potential of RGB and multispectral cameras on board an eight-rotor UAV to measure N status of rice plants from tillering to booting stages. However, only images on 1 day were used in their study and they used averaged band reflectance values over entire small plots of different treatments to build prediction models without separating rice plants from the backgrounds.

In order to better apply UAS to precision agriculture, the objectives of the study were to (1) extract band reflectance of rice plants only from images obtained from a multispectral camera mounted on a drone, (2) analyze relationships between various vegetation indices and ground truth data to determine the period best for assessment of N status through UAS, (3) develop a N status estimation model for the best period determined, and (4) demonstrate how to use the developed model through an actual case study.

Materials and methods

This study is divided into two parts, as shown in Fig. 1. In the first part, a model suitable for estimating plant nitrogen status in the vegetative phase was developed. In the second part of the study, SPAD value distribution maps at several DATs of an experimental field for fertilizer trials were generated as an example to illustrate how to employ the developed N estimation model.

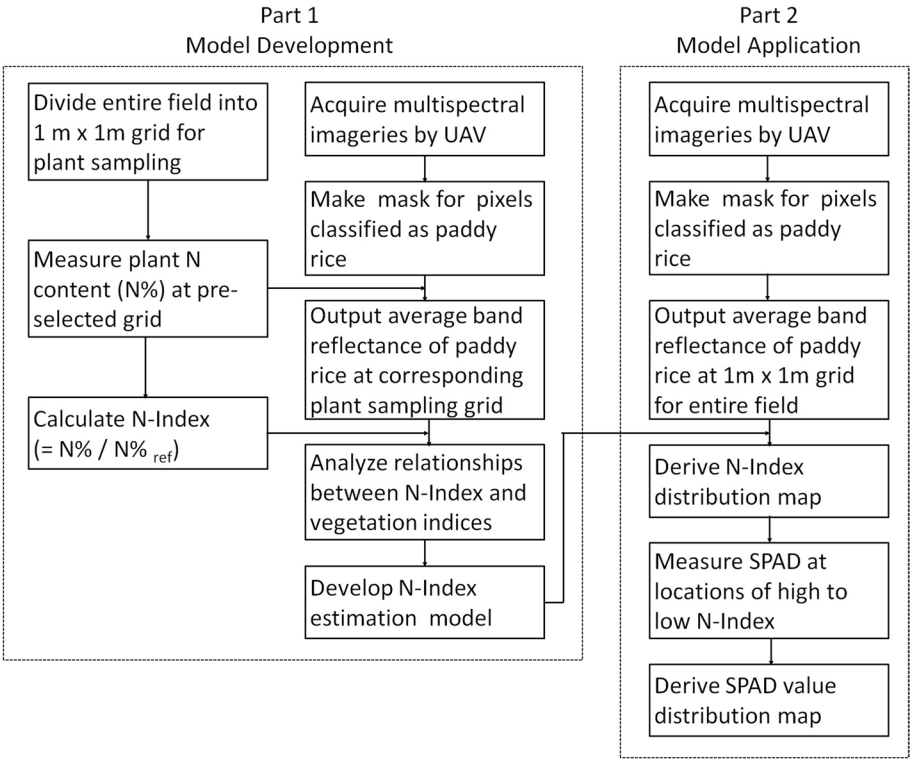

Fig. 1 Flow chart illustrates important steps employed in this study

Study site and experimental layout

Field experiments were conducted from 2018 to 2020 at the experimental farm of Taiwan Agricultural Research Institute (TARI) located at 24° 02′ N latitude and 120° 41′ E longitude at an altitude of 73 m above mean sea level. The climate of the study site is classified as Cwa by the Köppen system.

In Fig. 1, the part 1 of the study was conducted at field #80 at the vegetative phase of rice (*Oryza sativa*, L. cultivar TNG71) during the second crop season of 2018 and the first crop season of 2019. The field, 0.5 ha in size, was divided into eight 25 m × 25 m blocks. Four nitrogen application rates (0, 45, 90, 180 kg N ha^{-1}) with 2 replicates were assigned to each of these 8 blocks (Fig. 2a). Rice seedlings at three- to four-leaf stage were machine-transplanted, 3–5 plants per hill, at row spacing of 0.3 m and hill distance of 0.2 m. The transplanting dates were on July 23, 2018 and March 6, 2019, respectively. The nitrogen fertilizer applied was split into three doses; 55% of each amount was distributed as pre-planting basal 5 days before transplanting; 27% as the first top dressing applied 3 weeks (second crop) or 4 weeks (first crop) after transplanting; and the remaining 18% was added 20 days before heading. For all N treatments, adequate phosphate (146 kg P_2O_5 ha^{-1}) and potassium (90 kg K_2O ha^{-1}) fertilizers were also applied based on local recommendation; herbicides and pesticides were sprayed during rice growth as needed.

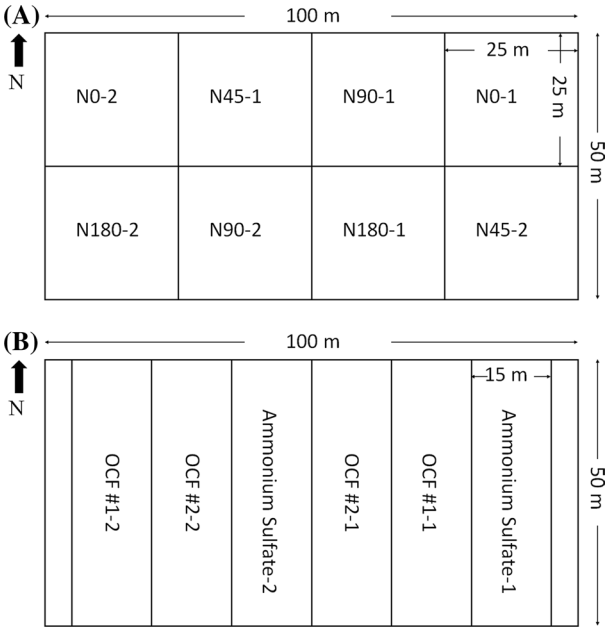

Fig. 2 Field experiment layout for **A** N-index model development and **B** N-index model application in this study

In Fig. 1, the part 2 of the study was conducted at field #50 at the vegetative phase of rice (*Oryza sativa*, L. cultivar TN11) during the first crop season of 2020. The field was divided into six equal-area blocks (15 m wide and 50 m long) laid out side-by-side to test the performance of two organic compound fertilizers (OCF #1 and #2) against the ammonium sulfate (AS). The three types of nitrogen fertilizers with 2 replicates were assigned to each of these 6 blocks (Fig. 2b). Rice seedlings at three- to four-leaf stage were transplanted on 24 February, 2020, 3–5 plants per hill, at row spacing of 0.3 m and hill distance of 0.2 m. All the nitrogen fertilizers, at the same rate of 180 kg N ha^{-1}, were split into four doses; 25% as pre-planting basal 5 days before transplanting; 20% as the first top dressing applied on DAT 15; 30% as the second top dressing applied on DAT 30; and the remaining 25% was added on DAT 45. Calcium superphosphate and potassium chloride, at rate of 175 kg P_2O_5 ha^{-1} and 100 kg K_2O ha^{-1}, respectively, were also applied in the ammonium sulfate plots as basal and top dressing in order to match the time and amount of phosphate and potassium added by OCF #1 and #2. Herbicides and pesticides were also sprayed during rice growth as needed.

UAV images acquisition and processing

A multispectral camera (RedEdge-M, MicaSense Inc., Seattle, WA, USA) mounted on a quadcopter UAV (Matrice 100, DJI Science and Technology Co., Ltd., Shenzhen, China) was used to collect the aerial images. The UAV flight operation was carried out between 10:00 to 11:00 local time and at an altitude of 50 m, which gave a ground sampling distance (GSD) of 14 mm. The UAV images were scheduled to be acquired on a weekly basis when the sky was clear and on DAT 30, DAT 45 and DAT 52 for part 1 and part 2 of this study, respectively.

A photogrammetry software (Pix4Dmapper, Pix4D Inc., San Francisco, CA, USA) was used to convert data from raw images to ortho-mosaic band reflectance maps by selecting the camera and sun irradiance option. Prior to other image analysis, pixels of the converted images were first classified into one of the five classes (i.e. rice plants, water, soil, algae, and others) by ISODATA method (ENVI, Harris Geospatial Solutions, Broomfield, CO, USA) based on the reflectance of the blue (B), green (G), red (R), red edge (RE) and near infrared (NIR) bands collected by the multispectral camera. The accuracy of classifying a pixel to rice plants was evaluated through visual inspection by comparing randomly selected 100 pixels classified as rice plants against the ortho-mosaic image. The accuracies in classifying the rice plants were higher than 90% for all images collected at various DATs and increased as the growth and development of rice plants became more apparent. A mask for rice plants was then built by assigning a value of 1 to pixels classified as rice plants and 0 to all other classes. Average band reflectance maps, at 1 m × 1 m grid, of rice plants only were obtained by multiplying the band reflectance maps by the rice plant mask and resampled by cubic spline method using functions provided by ENVI.

Field data collection

Plant sampling locations and sequence for part 1 of this study are shown in Fig. 3. In each of the eight blocks (4 N treatments × 2 replicates), there were six subdivided areas

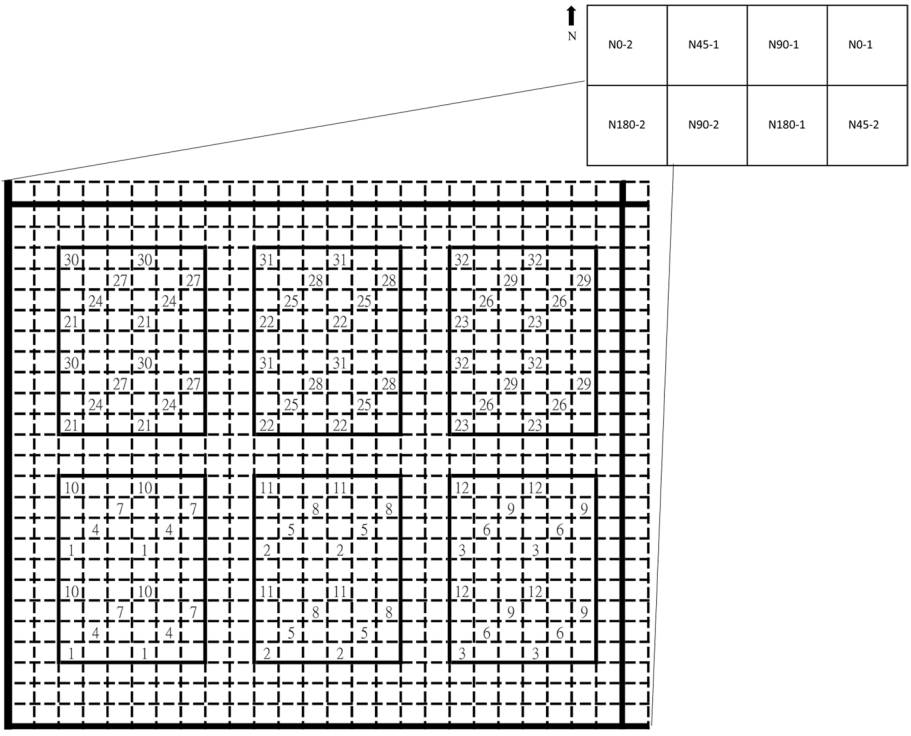

Fig. 3 Schematics showing the locations and sequence of plant sampling used in part 1 of this study. The six rectangles within each N treatment block illustrated the locations of the six subareas used for N-index model development (#1−#12) and validation (#21−#32)

and with number coded 1 m × 1 m grids in each sub-area. For model development, rice plant samples were taken from the three sub-areas (# 1 to #12) every week after transplanting in sequence from right to left. For example, plant samples were taken from the four #1 coded grids in the left sub-area for week 1 after transplanting, the four #2 coded grids in the center sub-area were sampled for week 2, and the four #4 coded grids in the left sub-area were sampled for week 4. The three sub-areas (# 21 to #32) in each block were for validation test and were sampled every 2 weeks after transplanting in a similar sequence as described above. During each sampling, five plants from the center and four corners of the 1 m × 1 m grid were collected to form the sample representing that grid.

Plant samples dried at 60 °C for 72 h were milled and passed through a 0.1 mm mesh to determine the total N content of the plants using the modified Kjeldahl method (Bremner, 1996). In order to resolve the problem of rapid changes in plant N content during the vegetative phase, N-index were calculated for each batch of plant samples using Eq. (1).

$$\text{N-index} = \text{N\%}/\text{N\%}_{\text{ref}} \tag{1}$$

where N% and $\text{N\%}_{\text{ref}}$ are N content of plants to be evaluated and plants not receiving N fertilizers, respectively.

For part 2 of this study, after each flight operation and N-index map derivation (to be described below), SPAD measurements (SPAD-502, Konica Minolta Inc., Osaka, Japan) were conducted at about 15 locations (composed of low to high N-index values) around the field to establish relations between estimated N-index and SPAD values. For each location, 10 SPAD readings were taken on the second uppermost fully expanded leaves, midway between the leaf base and tip. All readings were then averaged to represent that grid.

Model development and validation

Vegetation indices (VIs) examined for the development of N-index estimation models are listed in Table 1. Correlation analysis indicated that NDRI, RECI, MSAVI, CCVI, GNDVI and NDVI (in the order of decreasing values of correlation coefficients) had better Pearson's correlation coefficient ($|r| > 0.1$) with the N-index values than the rest of the VIs when polling all the data of 2018 and 2019 together (data not shown). Therefore, correlation coefficients between the observed N-index values against each of these six VIs were further computed for different period combinations through continuous removal of dates starting from the earliest DAT or the latest DAT. The widest period that had $|r| \geq 0.5$ was determined as the best period suitable for developing a N-index estimation model. Data pairs of N-index and VIs within the determined best period were then used to find independent variables for the required N-index estimation model through stepwise regression analysis with F to enter and F to remove set as 1 and 0, respectively (STATISTICA, TIBCO Software Inc., Palo Alto, CA, USA). To avoid overfitting problem of the stepwise regression method, various linear models based on different combinations of the selected VIs were tested against the validation dataset collected as described in the field data collection section. Root mean square error (RMSE) and mean bias error (MBE) were used as the basis to determine the best model for N-index estimation. The RMSE and MBE are defined as

Table 1 Spectral vegetation indices evaluated in this study

Vegetation Index (VI)	Abbrev	Equations[a]	References
Excess green	ExG	$(2G-R-B)/(R+G+B)$	Woebbecke et al. (1995)
Excess red	ExR	$(1.4R-G)/(R+G+B)$	Meyer et al. (1998)
Excess green minus excess red	ExGR	$ExG-ExR$	Meyer and Neto (2008)
Normalized Difference Index	NDI	$(G-R)/(G+R)$	Perez et al. (2000)
Visible Atmospheric Resistant Index	VARI	$(G-R)/(G+R-B)$	Gitelson et al. (2002)
Red-Green Index	RGI	R/G	Steele et al. (2009)
Chlorophyll Efficiency Vegetation Index	CEVI	NIR/G	Chang et al. (2005)
Simple Ratio Vegetation Index	SRVI	NIR/R	Lee et al. (2008)
Normalized Difference Vegetation Index	NDVI	$(NIR-R)/(NIR+R)$	Arai et al. (2014)
Green Normalized Difference Vegetation Index	GNDVI	$(NIR-G)/(NIR+G)$	Gitelson et al. (1996)
Enhanced Normalized Difference Vegetation Index	ENDVI	$(NIR+G-2B)/(NIR+G+2B)$	Zheng et al. (2018)
Modified Soil Adjusted Vegetation Index	MSAVI	$\frac{2NIR+1-\sqrt{(2NIR+1)^2-8(NIR-R)}}{2}$	Qi et al. (1994)
Normalized Difference Red edge Index	NDRI	$(NIR-RE)/(NIR+RE)$	Barnes et al. (2000)
Red Edge Chlorophyll Index	RECI	$NIR/RE-1$	Gitelson et al. (2003)
Chlorophyll Content Vegetation Index	CCVI	$(NIR-RE)/(NIR-R)$	Datt (1999)

[a]Band code B, G, R, RE and NIR represents blue, green, red, red edge, and near infrared band, respectively

$$\mathrm{RMSE} = \sqrt{\frac{1}{\mathrm{N}}\sum_{\mathrm{i}=1}^{\mathrm{N}}\left(\mathrm{P_i} - \mathrm{O_i}\right)^2} \tag{2}$$

$$\mathrm{MBE} = \frac{1}{\mathrm{N}}\sum_{\mathrm{i}=1}^{\mathrm{N}}\left(\mathrm{P_i} - \mathrm{O_i}\right) \tag{3}$$

where O and P represent observed and predicted values, and N is the total number of observations. The RMSE summarizes the mean difference in the units of observed and predicted values, with the zero indicating good and positive infinity considered as poor model performance. The MBE gives an idea of the degree of overestimating or underestimating of the model.

Results and discussion

Variations of plant nitrogen content with days after transplanting (DAT)

The variation of plant nitrogen content with DAT for different N treatments of two rice crop seasons are shown in Fig. 4. It started from approximately 2% after transplanting, increasing to approximately 4%, then decreasing to about 1% at the end of the vegetative phase. Plant nitrogen content increased with nitrogen fertilizer application rates. The observed pattern of changes in plant nitrogen content is the compound result of uptake of nitrogen released from soil and fertilizers and the amount of dry matter accumulated through photosynthesis. At the beginning of the vegetative phase, when the photosynthetic

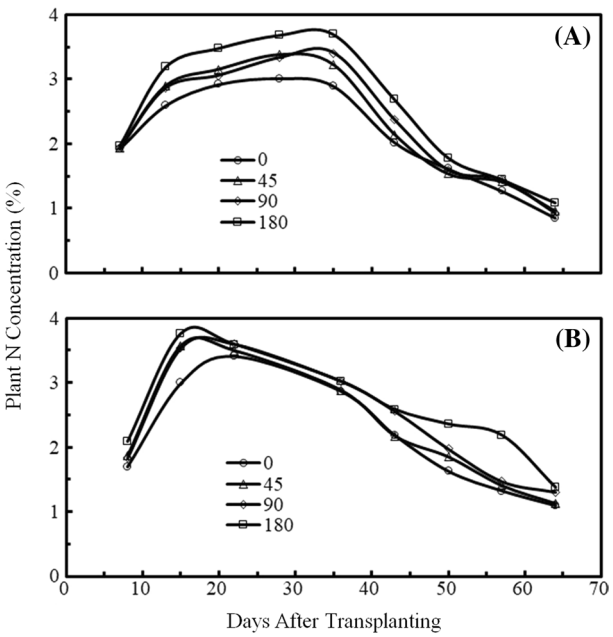

Fig. 4 Variations of plant nitrogen content with days after transplanting for **A** the second crop season of 2018, **B** the first crop season of 2019. The legends indicate nitrogen fertilizer application rates (kg N ha^{-1})

capacity is small, absorbed nitrogen resulted in an increase of plant nitrogen content. After recovery from transplanting shock, the leaf area index increased rapidly and resulted in a decrease of plant nitrogen content. However, the time that plant nitrogen content reached its peak varied with the crop season. Nitrogen uptake was reduced by the low temperatures at beginning of the first crop season (generally from end of February to June, i.e. from cool to warm environment), which resulted in reaching the peak earlier than the second crop season (generally from end of July to November, i.e. from warm to cool environment). Lee et al. (2011) also indicated that the nitrogen uptake was faster in plants grown during the second cropping season than during the first cropping season.

Variations of band reflectance of rice plants with nitrogen treatments and DAT

Leaf chlorophyll content altered the leaf transmittance and reflectance in the visible region (Blackmer et al., 1994). The increase in chlorophyll content as result of increasing in leaf area index with DAT tended to absorb more strongly in the visible region, which resulted in a decrease of reflectance at blue, green and red bands (Fig. 5).

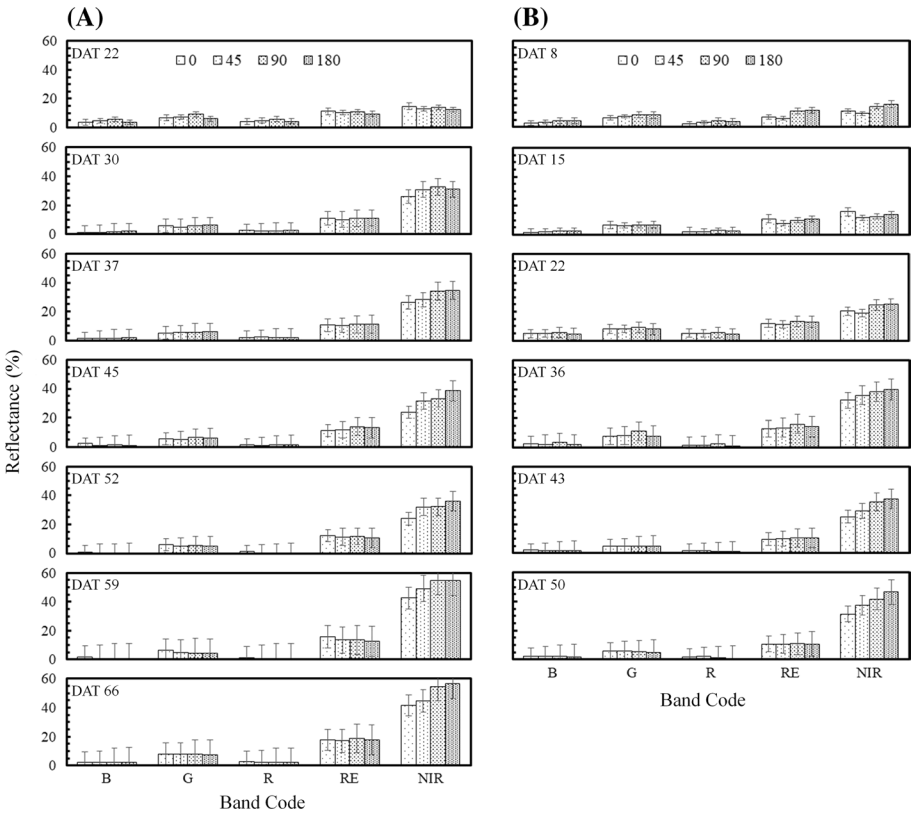

Fig. 5 Changes of band reflectance of rice plants with nitrogen treatments and days after transplanting (DAT) for **A** the second crop season of 2018 and **B** the first crop season of 2019. The band code B, G, R, RE and NIR represents blue, green, red, red edge, and near infrared band, respectively. The legends indicate nitrogen fertilizer application rates (kg N ha^{-1})

However, there were only slight differences between N treatments, making it difficult to distinguish with the naked eye.

Reflectance in the near-infrared region is related to the diffraction at air–liquid interface within the leaves, and is thus affected by internal leaf structure and canopy architecture, as well as increases in plant biomass (Guyot, 1990). Accordingly, the thicker and more turgid leaves of plants, due to higher N content, would reflect more strongly in the near infrared band (Fig. 5).

The increased absorption by chlorophyll and the reflection by thicker, flatter and more turgid leaves would result in a steeper slope of the reflectance spectrum in transition region between the red to near-infrared region. Therefore, Lee et al. (2008) used the derivative of reflectance between 730 and 740 nm, $dR/d\lambda|_{735}$, to account for changes in plant N content. The red edge band of the multispectral camera (RedEdge-M, MicaSense) measured averaged reflectance of a band that had a bandwidth of 10 nm and centered at 717 nm, which was not equal to the slope of the reflectance spectrum in the transition region between the red to near-infrared region. Thus, no significant differences in reflectance were observed between N treatments in the red edge band. In this regard, a hyperspectral imager may be a better sensor for plant N assessment.

Relationships among N-index, vegetation indices and DAT

To develop a linear regression model based on representative indices, a correlation matrix was developed between the N-index values and the six selected VIs at various time periods. Figure 6 shows the correlation levels between the N-index and each VI at the time period selected. For most VIs, except NDVI, data pairs in between DAT 30 and DAT 55 of the two rice cropping seasons showed modest ($r \geq 0.5$) linear relationships with N-index. This period covers the latter half of the vegetative phase, which is also the most important period to top dress the nitrogen fertilizers for better yield and grain quality (Nguyen & Lee, 2006).

At early stage of the vegetative phase (e.g. DAT 8 and 15), the poor correlation may be due to image classification errors because the rice plants were rather small and could not be easily separated from the background at the spatial resolution used. As growth stages reached the transition period from vegetative phase to reproductive phase (e.g. DAT 59 and 66), band reflectance of leaves may be over-weighted by using the rice mask due to overlapping of leaves as the percent cover reaches nearly 100%. To correct for the structural influences, hyperspectral reflectance spectra in the interval 710–790 nm are needed in order to generate corresponding directional area scattering factor (DASF) values (Knyazikhin et al., 2013). However, in this study, DASF could not be obtained due to limited bands of the multispectral camera used.

All six of the selected indices involve near infrared band which is related more to internal leaf structure and canopy architecture than leaf color. This is probably due to the fact that only minor differences were observed in the visible band and canopy structural parameters (e.g. LAI and biomass) are affected by the amount of N available, which corresponds with the findings in other studies (Lee et al., 2008; Zheng et al., 2018). Therefore, although an RGB camera usually comes with the UAV, it may be better to use a multispectral camera for plant nitrogen status monitoring.

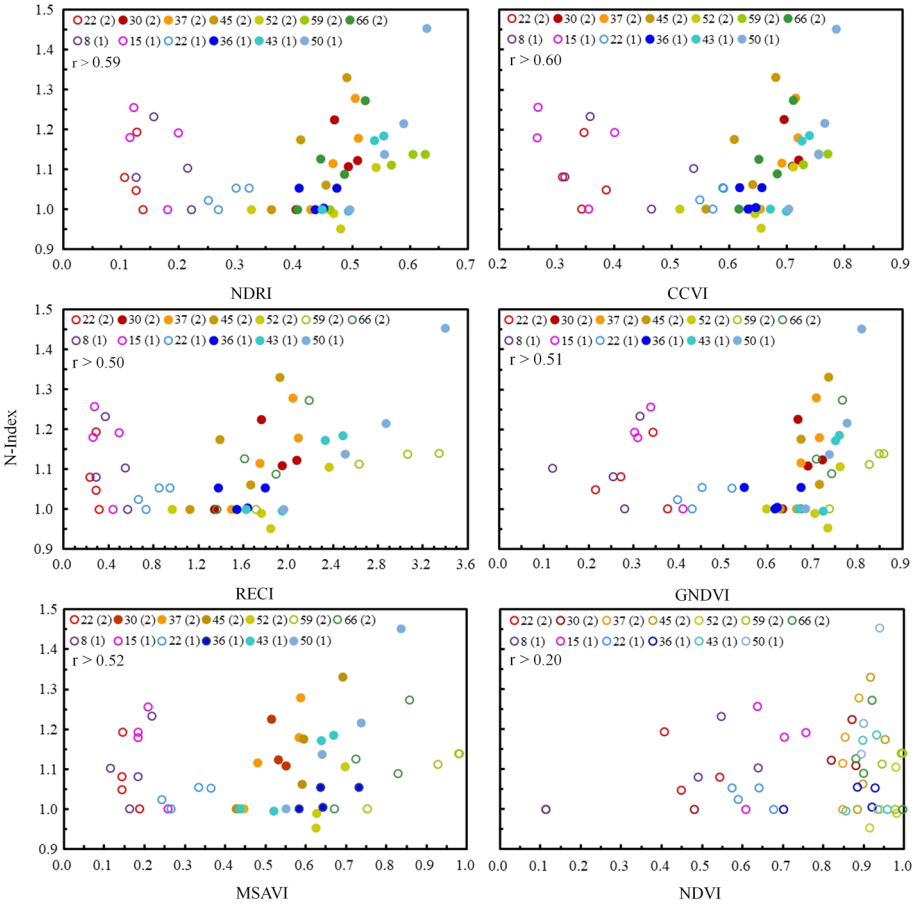

Fig. 6 Results of determining the best period for developing N-index estimation model. The top row of the legends is for the second crop season of 2018 and the bottom row is for the first crop season of 2019. Numbers indicates DAT and the filled legends represent dates included in the correlation coefficients (r) analysis

Development of regression model for N-index assessment

Five vegetation indices, NDRI, RECI, MSAVI, CCVI and GNDVI, were picked by the stepwise multiple regression analysis as independent variables to build the N-index estimation model. To avoid over-fitting the model, tests of the validation dataset against various combinations of these five vegetation indices indicated that a linear model based on NDRI and RECI (Eq. 4) gave the lowest RMSE (=0.061) compared with other combinations and overestimated only slightly (MBE=0.004).

$$\text{N-Index} = 1.188 + 0.356\,\text{RECI} - 1.586\,\text{NDRI} \quad R^2 = 0.49 \tag{4}$$

Figure 7 shows the scatterplot between estimated and measure N-index values. It can be seen from the validation results that the developed regression model performed well to

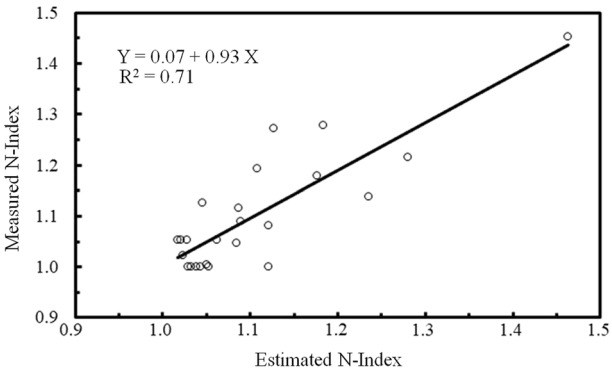

Fig. 7 Scatter plot between estimated and measured N-index for validation dataset

estimate the N-index values. Most of the estimated N-index values are within the range of ± 10% deviation from the 1:1 line.

Mapping nitrogen distribution in field

In part 2 of this study, UAV images of an experimental field at DAT 30, 45 and 52 of the first cropping season of 2020 were used to explore the spatial and temporal changes of plant nitrogen status in the field. Using the same scheme as in part 1, all the aerial raw images were converted to ortho-mosaic band reflectance maps by Pix4Dmapper (Pix4D Inc.) and classified into five classes (i.e. rice plants, water, soil, algae and others) by ISO-DATA method and with averaged band reflectance maps of rice plants at 1 m × 1 m generated by ENVI (Harris Geospatial Solutions).

Spatial maps of estimated N-index were then generated based on Eq. 4 using the band math function of ENVI, relationships between N-index and SPAD values for the three DATs studied and distribution maps of the SPAD values converted from the relations are shown in Fig. 8. Spatial and temporal heterogeneity was clearly observable in the field. In Fig. 8A and C, somewhat apparent linear streaks appeared in the N–S direction of the field at all three dates, which could be the result of manually top dressing the fertilizers in that direction, while the relatively lower N-index at the south end of the field could be due to the dilution of the applied fertilizers by irrigation water (irrigation water flows into each treatment plot from south end). In Fig. 8C, the decrease of SPAD values on DAT 45 compared with those on DAT 30 indicated gradual depletion of nitrogen nutrients in the field due to uptake by rice plants. After top dressing the nitrogen fertilizer on DAT 45, the SPAD values of rice plants increased again on DAT 52.

The SPAD maps, shown in Fig. 8C, provide the required information regarding the spatial distribution of nitrogen status in the field and could thus be used as a guide to variable rate application of nitrogen fertilizers by suitable machines (such as drones especially made for fertilization). Although the SPAD value is merely a good surrogate for nitrogen status of rice plants, an actual plant nitrogen content map for more precise application rate decisions could be easily created once an operational relationship between SPAD values and plant nitrogen content has been established. Future work will focus on building such an operational relationship.

More studies should also focus on testing the developed model across different varieties and stress levels related to leaf N concentration to improve the robustness and applicability

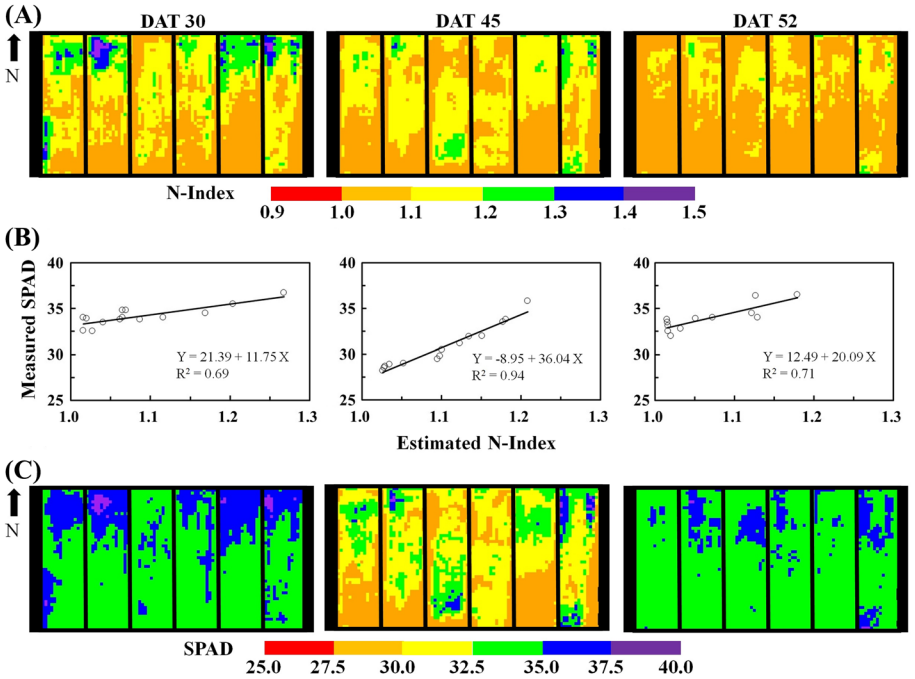

Fig. 8 Spatial distribution of N-index values (**A**), relationships between estimated N-index and measured SPAD values (**B**), and spatial distribution of SPAD values (**C**) at the fertilizers trial field on different days after transplanting (DAT)

of the model. Detailed studies regarding SPAD values and plant nitrogen content for different varieties and at different DAT are also needed for better site-specific and variable rate N management.

Conclusions

Due to the negative environmental and economic impacts of using conventional methods, there is growing interest over site-specific and variable rate nitrogen application. Remote sensing is emerging as an efficient tool for monitoring plant nitrogen status in the field. However, background (water, bare soil and algae) interferences created a mixed pixel problem when trying to extract nitrogen status information for rice plants at the vegetative phase. In the present study, background interferences were removed through using UAV-based high spatial resolution aerial images. Various vegetation indices of rice plants were calculated to evaluate their capability to monitor nitrogen status in rice crop. It was found that using a new variable, N-index (ratio of N content of plants to be evaluated and plants not receiving N fertilizers), can resolve the difficulty in developing a model to predict rapid changing of rice plant nitrogen content during vegetative phase. A linear regression model based on NDRI and RECI was developed for prediction of N-index at periods important in determining rice yield and grain quality, with RMSE and MBE of 0.061 and 0.004, respectively. Spatial maps of N-index and SPAD generated for the fertilizer trials field indicated

that the developed model has good potential to identify plant N status at the vegetative phase of paddy rice.

Acknowledgements This work was financially supported by the "Innovation and Development Center of Sustainable Agriculture" from the Featured Areas Research Center Program within the framework of the Higher Education Sprout Project by the Ministry of Education, and Ministry of Science and Technology, Taiwan, ROC [Grant Number MOST 106-2313-B-005-013-MY3].

Declarations

Conflict of interest The authors declare that they have no known competing financial interests or personal relationships that could have appeared to influence the work reported in this paper.

References

Arai, K., Shigetomi, O., Sakashita, M., & Miura, Y. (2014). Estimation of protein content in rice crop and nitrogen content in rice leaves through regression analysis with NDVI derived from camera mounted radio-control helicopter. *International Journal of Advanced Research in Artificial Intelligence, 3*, 12–19. https://doi.org/10.14569/IJARAI.2014.030303

Barnes, E. M., Clarke, T. R., Richards, S. E., Colaizzi, P. D., Haberland, J., Kostrzewski, M., et al. (2000). Coincident detection of crop water stress, nitrogen status and canopy density using ground based multispectral data. In *Proceedings of the Fifth International Conference on Precision Agriculture*, ASA/SSSA/CSSA, (Vol. 1619).

Blackmer, T. M., Schepers, J. S., & Varvel, G. E. (1994). Light reflectance compared with other nitrogen stress measurements in corn leaves. *Agronomy Journal, 86*, 934–938. https://doi.org/10.2134/agronj1994.00021962008600060002x

Bremner, J. M., et al. (1996). Nitrogen-total. In D. L. Sparks (Ed.), *Methods of soil analysis. Pt 3. Chemical methods. SSSA Book Ser. 5,* (pp. 1085–1122). SSSA and ASA.

Buresh, R. J., Castillo, E. G., & De Datta, S. K. (1993). Nitrogen losses in puddle soils as affected by timing of water deficit and nitrogen fertilizer. *Plant and Soil, 157*, 197–206. https://doi.org/10.1007/BF00011048

Cabangon, R. J., Castillo, E. G., & Tuong, T. P. (2011). Chlorophyll meter-based nitrogen management of rice grown under alternate wetting and drying irrigation. *Field Crops Research, 121*, 136–146. https://doi.org/10.1016/j.fcr.2010.12.002

Cassman, K. G., Dobermann, A., & Walters, D. T. (2002). Agroecosystems, nitrogen-use efficiency, and nitrogen management. *Ambio, 31*, 132–140. https://doi.org/10.1579/0044-7447-31.2.132

Chang, K. W., Shen, Y., & Lo, J. C. (2005). Predicting rice yield using canopy reflectance measured at booting stage. *Agronomy Journal, 97*, 872–878. https://doi.org/10.2134/agronj2004.0162

Datt, B. (1999). Visible/near infrared reflectance and chlorophyll content in Eucalyptus leaves. *International Journal of Remote Sensing, 20*, 2741–2759. https://doi.org/10.1080/014311699211778

Galloway, J. N., & Cowling, E. B. (2002). Reactive nitrogen and the world: 200 years of change. *Ambio, 31*, 64–71. https://doi.org/10.1579/0044-7447-31.2.64

Gitelson, A. A., Kaufman, Y. J., & Merzlyak, M. N. (1996). Use of green channel in remote sensing of global vegetation from EOS-MODIS. *Remote Sensing of Environment, 58*, 289–298. https://doi.org/10.1016/S0034-4257(96)00072-7

Gitelson, A. A., Gritz, Y., & Merzlyak, M. N. (2003). Relationships between leaf chlorophyll content and spectral reflectance and algorithms for non-destructive chlorophyll assessment in higher plant leaves. *Journal of Plant Physiology, 160*, 271–282. https://doi.org/10.1078/0176-1617-00887

Gitelson, A. A., Stark, R., Grits, U., Rundquist, D., Kaufman, Y., & Derry, D. (2002). Vegetation and soil lines in visible spectral space: A concept and technique for remote estimation of vegetation fraction. *International Journal of Remote Sensing, 23*, 2537–2562. https://doi.org/10.1080/01431160110107806

Guyot, G. (1990). Optical properties of vegetation canopies. In M. D. Steven & J. A. Clark (Eds.), *Applications of remote sensing in agriculture* (pp. 19–43). Butterworths.

Ju, X. T., Kou, C. L., Zhang, F. S., & Christie, P. (2006). Nitrogen balance and groundwater nitrate contamination: Comparison among three intensive cropping systems on the North China plain. *Environmental Pollution, 143*, 117–125. https://doi.org/10.1016/j.envpol.2005.11.005

Kalra, Y. P. (1998). *Hand book of reference methods for plant analysis* (pp. 75–92). CRC Press. https://doi.org/10.1201/9780367802233

Keshava, N., & Mustard, J. F. (2002). Spectral unmixing. *IEEE Signal Processing Magazine, 19*, 44–57. https://doi.org/10.1109/79.974727

Knyazikhin, Y., Schull, M. A., Stenberg, P., Mõttus, M., Rautiainen, M., Yang, Y., et al. (2013). Hyperspectral remote sensing of foliar nitrogen content. *Proceedings of the National Academy of Sciences, 110*, 185–192. https://doi.org/10.1073/pnas.1210196109

Lee, Y. J., Chang, K. W., Shen, Y., Huang, D. M., & Tsay, H. L. (2007). A handy imaging system for precision agriculture studies. *International Journal of Remote Sensing, 28*, 4867–4876. https://doi.org/10.1080/01431160601075566

Lee, Y. J., Yang, C. M., Chang, K. W., & Shen, Y. (2008). A simple spectral index using reflectance of 735 nm to assess nitrogen status of rice canopy. *Agronomy Journal, 100*, 205–212. https://doi.org/10.2134/agronj2007.0018

Lee, Y. J., Yang, C. M., Chang, K. W., & Shen, Y. (2011). Effects of nitrogen status on leaf anatomy, chlorophyll content and canopy reflectance of paddy rice. *Botanical Studies, 52*, 295–303.

Lin, F. F., Qiu, L. F., Deng, J. S., Shi, Y. Y., Chen, L. S., & Wang, K. (2010). Investigation of SPAD meter-based indices for estimating rice nitrogen status. *Computers and Electronics in Agriculture, 71*, S60–S65. https://doi.org/10.1016/j.compag.2009.09.006

Muñoz-Huerta, R. F., Guevara-Gonzalez, R. G., Contreras-Medina, L. M., Torres-Pacheco, I., Prado-Olivarez, J., & Ocampo-Velazquez, R. V. (2013). A review of methods for sensing the nitrogen status in plants: Advantages, disadvantages and recent advances. *Sensors, 13*, 10823–10843. https://doi.org/10.3390/s130810823

Meyer, G. E., & Neto, J. C. (2008). Verification of color vegetation indices for automated crop imaging applications. *Computers and Electronics in Agriculture, 63*, 282–293. https://doi.org/10.1016/j.compag.2008.03.009

Meyer, G.E., Hindman, T.W. & Lakshmi, K. (1998). Machine vision detection parameters for plant species identification. In: Meyer, G.E., & DeShazer, J.A. (Eds.), Precision agriculture and biological quality (vol. 3543, pp. 327–335). Proceedings of SPIE. https://doi.org/10.1117/12.336896

Nguyen, H. T., & Lee, B. W. (2006). Assessment of rice leaf growth and nitrogen status by hyperspectral canopy reflectance and partial least square regression. *European Journal of Agronomy, 24*, 349–356. https://doi.org/10.1016/j.eja.2006.01.001

Perez, A. J., Lopez, F., Benlloch, J. V., & Christensen, S. (2000). Color and shape analysis techniques for weed detection in cereal fields. *Computers and Electronics in Agriculture, 25*, 197–212. https://doi.org/10.1016/S0168-1699(99)00068-X

Qi, J., Chehbouni, A., Huete, A. R., Kerr, Y. H., & Sorooshian, S. (1994). A modified soil adjusted vegetation index. *Remote Sensing of Environment, 48*, 119–126. https://doi.org/10.1016/0034-4257(94)90134-1

Raun, W. R., Solie, J. B., Johnson, G. V., Stone, M. L., Mullen, R. W., Freeman, K. W., et al. (2002). Improving nitrogen use efficiency in cereal grain production with optical sensing and variable rate application. *Agronomy Journal, 94*, 815–820. https://doi.org/10.2134/agronj2002.0815

Steele, M. R., Gitelson, A. A., Rundquist, D. C., & Merzlyak, M. N. (2009). Nondestructive estimation of anthocyanin content in grapevine leaves. *American Society for Enology and Viticulture, 60*, 87–92.

Stroppiana, D., Boschetti, M., Brivio, P. A., & Bocchi, S. (2009). Plant nitrogen concentration in paddy rice from field canopy hyperspectral radiometry. *Field Crops Research, 111*, 119–129. https://doi.org/10.1016/j.fcr.2008.11.004

Wang, Y. P., Chang, K. W., Chen, R. K., Lo, J. C., & Shen, Y. (2010). Large area rice yield forecasting using satellite imageries. *International Journal of Applied Earth Observation and Geoinformation, 12*, 27–35. https://doi.org/10.1016/j.jag.2009.09.009

Wang, Y. P., Chen, S. H., Chang, K. W., & Shen, Y. (2012). Identifying and characterizing yield limiting factors in paddy rice using remote sensing yield maps. *Precision Agriculture, 13*, 553–567. https://doi.org/10.1007/s11119-012-9266-5

Wang, Y. P., & Shen, Y. (2015). Identifying and characterizing yield limiting soil factors with the aid of remote sensing and data mining techniques. *Precision Agriculture, 16*, 99–118. https://doi.org/10.1007/s11119-014-9365-6

Wang, Z., Zhang, W., Beebout, S. S., Zhang, H., Liu, L., Yang, J., et al. (2016). Grain yield, water and nitrogen use efficiencies of rice as influenced by irrigation regimes and their interaction with nitrogen rates. *Field Crops Research, 193*, 54–69. https://doi.org/10.1016/j.fcr.2016.03.006

Woebbecke, D. M., Meyer, G. E., Von Bargen, K., & Mortensen, D. A. (1995). Color indices for weed identification under various soil, residue, and lighting conditions. *Transactions of the ASAE, 38*, 259–269. https://doi.org/10.13031/2013.27838

Ye, Y., Liang, X., Chen, Y., Liu, J., Gu, J., Guo, R., et al. (2013). Alternate wetting and drying irrigation and controlled-release nitrogen fertilizer in late-season rice. Effects on dry matter accumulation, yield, water and nitrogen use. *Field Crops Research, 144*, 212–224. https://doi.org/10.1016/j.fcr.2012.12.003

Zheng, H., Cheng, T., Li, D., Zhou, X., Yao, X., Tian, Y., et al. (2018). Evaluation of RGB, color-infrared and multispectral images acquired from unmanned aerial systems for the estimation of nitrogen accumulation in rice. *Remote Sensing, 10*, 824. https://doi.org/10.3390/rs10060824

Zhu, Y., Yao, X., Tian, Y., Liu, X., & Cao, W. (2008). Analysis of common canopy vegetation indices for indicating leaf nitrogen accumulations in wheat and rice. *International Journal of Applied Earth Observation and Geoinformation, 10*, 1–10. https://doi.org/10.1016/j.jag.2007.02.006

Publisher's Note Springer Nature remains neutral with regard to jurisdictional claims in published maps and institutional affiliations.